

# Crystallographic structure of ultrathin Fe films on Cu(100)

Albert Biedermann, Rupert Tscheließnig, Michael Schmid, and Peter Varga  
*Institut für Allgemeine Physik, Vienna University of Technology, A-1040 Vienna, Austria*

We report bcc-like crystal structures in 2–4 ML Fe films grown on fcc Cu(100) using scanning tunneling microscopy. The local bcc structure provides a straightforward explanation for their frequently reported outstanding magnetic properties, i.e., ferromagnetic ordering in all layers with a Curie temperature above 300 K. The non-pseudomorphic structure, which becomes pseudomorphic above 4 ML film thickness is unexpected in terms of conventional rules of thin film growth and stresses the importance of finite thickness effects in ferromagnetic ultrathin films.

Both academic interest in novel nanomagnetic phenomena as well as their technological importance for magneto-electronics and high density magnetic storage devices make the study of ultrathin ferromagnetic films particularly worthwhile. These extremely thin films, typically less than 10 monolayers (ML) thick, exhibit significantly different magnetic properties in contrast to the bulk material, e.g., different magnetization directions, enhanced magnetic moments, and lower Curie temperatures. Fe films epitaxially grown on Cu(100) are distinguished by a particular complex behavior since they are variable both with respect to magnetic ordering (ferro- or antiferromagnetic) and crystal structure (fcc or bcc). Although the epitaxial system Fe/Cu(100) is under intense scrutiny for more than a decade and its magnetic properties have been mapped very precisely, no conclusive overall picture of the relation between structure and magnetic states has emerged yet. Regarding the model for films deposited at room temperature presently discussed in the literature, there is clear evidence for an antiferromagnetic, pseudomorphic fcc phase between 5 and 10 ML film thickness. The character and origin of the ferromagnetic phase between 2 and 4 ML, however, remains unclear. Low energy electron diffraction (LEED) [1], surface extended X-ray absorption fine-structure (SEXAFS) [2], and medium energy ion scattering studies (MEIS) [3] indicate a distinct distortion of the fcc lattice in 2–4 ML films. This reconstruction, which is considered to comprise the entire film thickness [1], is accompanied by a substantial increase of the film volume (interlayer distance) by about 5% [1,4]. In the past, these results led to the notion of a second, ferromagnetic fcc-like phase with an expanded film volume, i.e., a face centered tetragonal (fct) phase. While *ab-initio* calculations of bulk Fe do support the possibility of a ferromagnetic fcc phase with expanded volume under substantial tensile strain [5], the respective calculations of ultrathin films on Cu(100) did not provide an unambiguous confirmation of the ferromagnetic fct model [6,7]. This is an important question since the hypothetical existence of a ferromagnetic fcc-like phase is relevant also for the solid state physics of Fe. The two- $\gamma$ -state model introduced by Kaufman, Clougherty, and Weiss [8], assuming two fcc states of bulk Fe either ferro- or antiferromagnetic, is still under discus-

sion.

In this Letter, we resolve this issue by characterizing the atomic structure of the ultrathin films below 5 ML thickness locally by scanning tunneling microscopy (STM). The key result is the characteristic bcc-like nature of the films, which pinpoints the true source of ferromagnetism in ultrathin Fe films on Cu(100), and reveals the actual root of this phenomenon: The remarkable stability of a non-pseudomorphic bcc-like phase in a film only 2–4 ML thick, while above 4 ML the pseudomorphic fcc structure is more stable.

The Fe films were grown on a (100) oriented Cu single crystal at 310 K (except the 2.5 ML film grown at 130 K and annealed to 300 K) by evaporation from tips of Fe wires in ultra-high vacuum using a deposition rate around 1 ML/min. The evaporator was calibrated using a quartz crystal microbalance and the film thickness checked by quantitative Auger electron spectroscopy [9]. Imaging was done using either a room temperature scanning tunneling microscope (STM) or a low temperature STM operated at 80 K with *in situ* sputtered W tips. Ion scattering experiments show that the surfaces of films more than 3 ML thick deposited at room temperature contain less than a few percent copper [10].

Before we report on the atomic structure of the films, a general remark: It is well known from previous experiments that the atomic structure can change within fractions of a monolayer and also with temperature [1,11]. Since it is very difficult to obtain atomic resolution on these surfaces, we did not attempt to outline the boundaries in the phase diagram by STM, which has been done before by means of LEED and the surface magneto-optical Kerr effect [1,12,13], but rather focused on the principal structures and driving forces, which support ferromagnetism in the 2–4 ML films.

After preparation of several films in the thickness range between 2 and 4 ML, and resolving the surface atomically either at 300 or 80 K we always observed a rather complex microdomain pattern of  $(1 \times 4)$ ,  $(1 \times 5)$ , and  $(1 \times 6)$  structures coexisting with remnants of the fcc structure. The STM images in Fig. 1 reveal the atomic structure of the respective unit cells. All structures can be imagined as resulting from shearing the fcc lattice by  $14^\circ$ , which makes the local atomic arrangement very similar to that

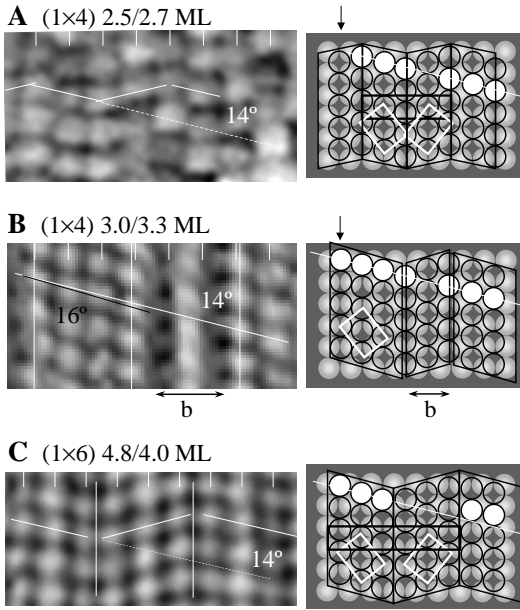


FIG. 1. Atomically resolved STM images of 2–4 ML films. (A)  $(1 \times 4)$  structure; Film grown at 80 K, annealed at 300 K, and imaged at 80 K. (B)  $(1 \times 4)$ -like structure with boundary “b”; Film grown at 310 K and imaged at 80 K. (C)  $(1 \times 6)$  structure; Film grown at 310 K and measured at 310 K. The width of the either  $+14^\circ$  or  $-14^\circ$  sheared bcc-like stripes varies between 2 and 4 atom rows. The first thickness value given was measured with a quartz crystal microbalance, the second by AES.

of a  $(110)$  oriented bcc film in the Pitsch orientation with respect to the fcc substrate [14] (see white unit cells in Fig. 1). The atomic surface density, however, is equal to that of the fcc(100) substrate, indicating a substantial strain in the bcc(110) film, whose surface density in the relaxed state is about 12% higher. Strictly speaking, the structures do not show the long range translational symmetry of a bcc lattice. Nevertheless, it will be shown quantitatively using linear elasticity theory that the local structure of the film is clearly bcc-derived and we will refer to it as “bcc-like”. Although there seems to be a large variety of structures, all of them consist of alternating sequences of stripes of bcc-like twins, leading to a zigzag-like deformation of the originally straight atom rows. The different structures are distinguished mainly by the width of their constituting bcc-like stripes. The  $(1 \times 4)$  structure seen in 2.5 ML films (2.7 ML AES) grown and imaged at 80 K consists of stripes only 2 rows wide, which makes it most compatible with the substrate lattice—only every second atom row is shifted by a quarter of the surface lattice constant. In general, the ordering in this film was low and it contained a mixture of fcc  $(1 \times 1)$ ,  $(1 \times 2)$ ,  $(1 \times 4)$ , and  $(1 \times 5)$  unit cells. The slightly more ordered structure in 3.0 ML (3.3 ML AES) films, which show the highest bcc-like content of all studied films, significantly more than 50%, contains

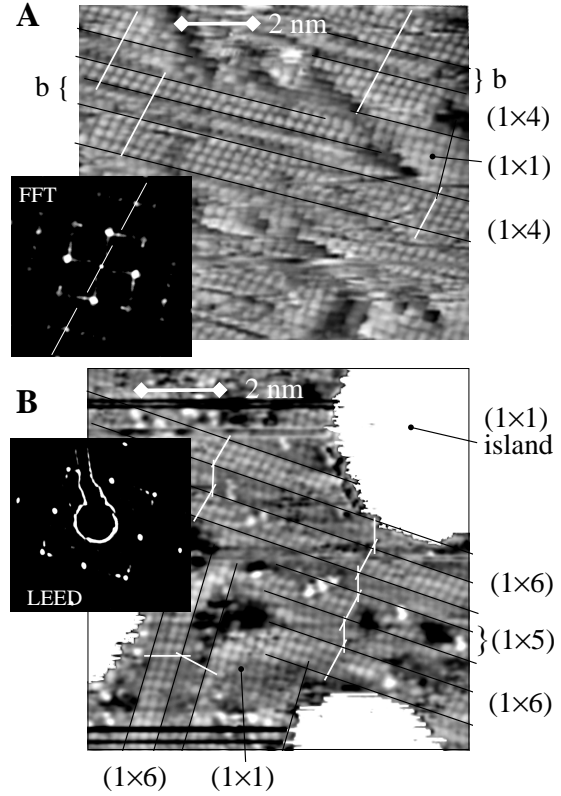


FIG. 2. STM images of films grown at 310 K, showing their microdomain structure. The black lines indicate the aligned fcc $\langle 100 \rangle$ /bcc $\langle 111 \rangle$  directions; the white lines mark the alternate bcc $\langle 111 \rangle$  directions, which are tilted by  $\sim 14^\circ$  with respect to the fcc $\langle 100 \rangle$  directions. (A) 3.0 ML film (3.3 ML AES) imaged at 80 K:  $(1 \times 4)$ -like stripes disrupted by boundaries “b” and small  $(1 \times 1)$  patches. The film is predominantly bcc-like. For details regarding the FFT image see text. (B) 4.8 ML film (4.0 ML AES) imaged at 300 K:  $(1 \times 6)$  domains embedded in a predominantly  $(1 \times 1)$  surface. The LEED pattern was acquired at 166 eV.

also 4 rows wide and occasionally even wider bcc-like stripes. These wider stripes can be easily generated from the “narrow-striped”  $(1 \times 4)$  lattice by shifting a hollow-site row by half the surface lattice constant (arrows in Fig. 1A,B). They show indications of local stress relaxation (see tick marks in Fig. 1B): The distance between the atom rows appears to contract while the shear angle increases slightly to  $16^\circ$ . The narrow separating boundaries (marked “b” in Fig. 1B, 2A) appear blurred, which might be due to an asymmetric STM-tip or a different crystal structure of the boundaries. In any case, these boundaries do not disturb the in-phase relationship of neighboring equally sheared stripes typical for the  $(1 \times 4)$  structure (see filled white atoms in Fig. 1 and white lines in Fig. 2). This is confirmed by the Fourier transformation (FFT) of the larger STM image displayed in Fig. 2A, which shows clear  $(1 \times 4)$  satellites to the principal  $(1,0)$  spots on one side. (In order to render the FFT more like a LEED image, we artificially overlaid the FFT of the same but  $90^\circ$  rotated image to simulate a mixed ro-

tational domain structure.) In contrast, the  $(1 \times 5)$  and  $(1 \times 6)$  structures, which dominate in thicker films, consist of bcc-like stripes two and three atoms wide. In the STM images of a 4.8 ML film (4.0 ML AES) displayed in Fig. 1C and 2B, the zigzag-like bcc structure exists only in the island-free regions and comprises only about 30% of the total film, whereas the surface of the monoatomic islands is pure fcc. The high fcc content indicates the close proximity to the transition thickness between the zigzag-like bcc and the fcc phase. By combining bcc-like stripes two and three atoms wide, which occurs in domain boundaries of the  $(1 \times 6)$  structure (see Fig. 2B), but has been seen also in larger domains, a  $(1 \times 5)$  structure is formed.

Concluding this brief structural survey, we find that while all structures are fairly similar, the films around 3.0 ML, which showed high magnetization in previous studies [1,12,13], have the highest bcc-like content and form the widest bcc-like stripes, whereas the films close to 2 and 5 ML show more narrow bcc-like stripes and high fcc content, respectively, which indicates a clear correlation of the bcc-like structure and the magnetization. The characteristic twin structure of these zigzag-like bcc phases combines local bcc order with a good lattice matching at the fcc substrate interface and a mass-transfer-free fcc-bcc transition pathway, the hallmarks of bulk martensitic transitions (see, e.g., Ref. [15]), only on much smaller length scales. Therefore, these novel bcc-like crystal structures may be termed “nano-martensitic bcc”.

Some aspects of the zigzag-like deformation of the fcc lattice resemble the sinusoidal deformation model proposed by Müller *et al.* [1], which was derived from I/V LEED data, but was 2–3 times smaller in the lateral amplitude. The much stronger zig-zag-like distortion of  $\pm 0.065$  nm (quarter of surface lattice constant of 0.255 nm) found by us is qualitatively different as it represents a phase transition to a different, i.e., bcc-like crystal structure. So far, the multi-phase microdomain structure and the incomplete reconstruction for most film thicknesses have apparently prevented the detection of the local bcc order by LEED [1], SEXAFS [2] or other surface averaging experiments.

An important issue in studies of this type is the subsurface structure of the films. STM can provide important hints by its sensitivity for the vertical relaxation of individual atoms (buckling). A single mismatched layer always causes the surface atoms to assume different vertical positions since the in-plane surface bonds and the subsurface back-bonds are equally important. The bcc-like stripes in our images, however, are either very flat or show height patterns that are incompatible with the assumption of an fcc layer directly underneath. Typically, larger domains of the  $(1 \times 6)$  structure show a “zebra-stripe” pattern (see Fig. 2B) with alternating bright and dark bcc-like twins, each 3 atoms wide (separated by

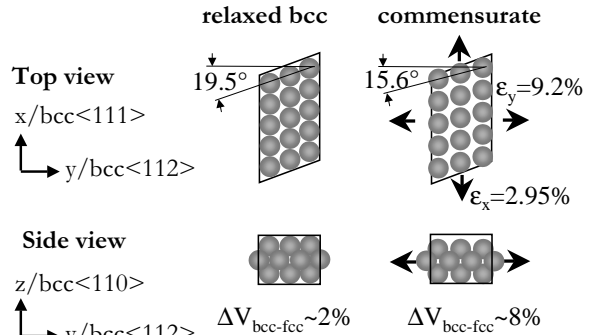


FIG. 3. The strained bcc film from the standpoint of linear elasticity theory: The shear angle [with respect to the orthogonal fcc(100) lattice] is reduced to  $15.6^\circ$  on exposure to a lateral biaxial strain of  $\varepsilon_y = 9.2\%$  and  $\varepsilon_x = 2.95\%$ , which is required to make the bcc structure commensurate to the substrate. The volume increase of the commensurate bcc-like film with respect to the pseudomorphic fcc film amounts to 8%.

black lines in Fig. 2B), with a difference in apparent height of about 10–20 pm, which we tentatively assign to subtleties of the stacking pattern of the zigzag-like structure.

The particular value of the shear angle of  $\sim 14^\circ$  visible in our STM images can be explained by the elastic properties of a bcc film and emphasizes the close relationship between the nanomartensitic bcc phase in the 2–4 ML films and the relaxed bcc structure. Figure 3 illustrates the effect of the biaxial strain of  $\varepsilon_y = 9.2\%$  and  $\varepsilon_x = 2.95\%$ , which is required to make the bcc film commensurate, calculated by linear elasticity theory using the anisotropic elastic constants for bcc Fe [16]. An immediately visible consequence is the reduction of the shear angle from its ideal value of  $19.5^\circ$  to  $15.6^\circ$ , which is close to our experimental value of  $\sim 14^\circ$ . Therefore, we conclude that the structure we observe is clearly bcc, although significantly strained.

Previous LEED studies [1,4,11] also indicate a volume expansion by about 5–6%, which was taken as a signature of a ferromagnetic fcc phase, predicted for strongly strained bulk fcc Fe [5]. Within our structural model, however, the full volume increase can be readily explained on the basis of linear elasticity theory. The high in-plane strain (cf. Fig. 3) leads to a volume (interlayer distance) of the strained bcc film, which is about 8% larger than the respective value of a commensurate fcc Fe film (1% strained [17]). This agrees well with the cited LEED data, if a small fcc admixture is included.

In order to fully appreciate the outstanding character of the nano-martensitic bcc structures in 2–4 ML films and to isolate possible driving forces, it is necessary to distinguish them from the nucleation of the precursors of the “regular” bcc phase in thicker films. These precursors appear as bcc needles in fcc films more than 5 ML thick and are clearly related to the tendency of “thick” fcc

films to assume the native bcc bulk structure [18]. There, the transformation to the bcc structure occurs because the film volume is large enough to generate sufficient energy to overcome the barrier due to the lattice mismatch, which is created in the course of the fcc to bcc transition. Moreover, since these bcc needles are only 8 atom rows wide, the fcc environment can relax the strain in the bcc needles somewhat, shifting the energy balance in favor of the bcc structure. In contrast, the larger defect-free bcc-like areas in the 2-4 ML films (e.g., Fig. 2B) have only half the volume (thickness) and additionally cannot relax the strain equally well. To enable the phase transition in these 2-4 ML films, an additional energy contribution is necessary. At least two finite size effects may contribute to this energy:

(1) Magnetic energy: It is known that surfaces and thin films show an increased tendency towards magnetism. For example, first principles calculations indicate a significant increase of the magnetic moment in particular for Fe surfaces, which contributes to their low surface energies [19]. Since the magnetic moment is enhanced not only in the surface layer but also in the layers adjacent to the Cu interface, the “bulk” of 2-4 ML bcc films is magnetically very different from bulk Fe (cf. also Refs. [6,7] for fcc films). Indeed, spin-polarized x-ray appearance-potential spectroscopy shows an increase of the spin asymmetry in 2.5 ML films on Cu(100) of about 12% with respect to 17 ML films or the surface of bulk samples [20].

(2) Magnetic entropy: The subtle balance between fcc and bcc in thin films is reminiscent of the entropy-driven bcc-fcc phase transitions in bulk Fe at higher temperatures. In bulk Fe the high temperature bcc phase ( $\delta$ ) is stabilized above 1665 K due to the rapid increase of magnetic disorder entropy around the bcc Curie temperature of 1040 K [21,22]. In 3 ML films the Curie temperature is only 380 K [12], which might lead to a decrease of the bcc free energy (via disorder entropy) by a few meV [22] in the 3 ML room temperature films already at room temperature.

To date, the available experimental and simulation data are insufficient to unambiguously explain the bcc-like phases in the 2-4 ML films. Nevertheless, we favor an enhanced magnetic energy as driving force as this contribution can easily generate sufficient energy to compensate the mismatch effects in the ultrathin bcc-like films.

In summary, we have observed bcc-like ( $1 \times n$ ) phases of Fe in ultrathin films below 5 ML film thickness. All structures consist of narrow stripes of strained bcc twins mostly 2-4 atom rows wide. This nano-martensitic bcc structure provides a natural explanation for the previously reported ferromagnetic character of these films. The volume (interlayer) expansion, which originally was the key argument to motivate a ferromagnetic fcc-like phase, is now explained as an elastic effect due to the strongly anisotropic strain state of the commensurate

bcc-like film. The surprising stability of a bcc-like phase in a regime that was expected to be predominantly pseudomorphic fcc stresses the importance of finite film thickness and/or finite temperature effects in these ultrathin films.

We gratefully acknowledge support by the “Fonds zur Förderung der Wissenschaftlichen Forschung” (Austrian Science Foundation) under project number Y75-PHY.

- 
- [1] S. Müller, P. Bayer, C. Reischl, K. Heinz, B. Feldmann, H. Zillgen, and M. Wuttig, *Phys. Rev. Lett.* **74**, 765 (1995).
  - [2] H. Magnan, D. Chandesis, B. Villette, O. Heckmann, and J. Lecante, *Phys. Rev. Lett.* **67**, 859 (1991).
  - [3] J. V. Barth and D. E. Fowler, *Phys. Rev. B* **52**, 11432 (1995).
  - [4] A. Clarke, P. J. Rous, M. Arnott, G. Jennings, and R. F. Willis, *Surf. Sci.* **192**, L843 (1987).
  - [5] V. L. Moruzzi, P. M. Marcus, K. Schwarz, and P. Mohn, *Phys. Rev. B* **34**, 1784 (1986).
  - [6] E. G. Moroni, G. Kresse, and J. Hafner, *J. Phys.: Condens. Matter* **11**, L35 (1999).
  - [7] D. Spišák and J. Hafner, *Phys. Rev. B* **61**, 16129 (2000).
  - [8] L. Kaufman, E. Clougherty, and R. J. Weiss, *Acta Met.* **11**, 323 (1963).
  - [9] P. J. Cumpson and M. P. Seah, *Surf. Interface Analysis* **25**, 430 (1997).
  - [10] T. Detzel, N. Memmel, and T. Fauster, *Surf. Sci.* **293**, 227 (1993).
  - [11] M. Zharnikov, A. Dittschar, W. Kuch, C. M. Schneider, and J. Kirschner, *J. Magn. Magn. Mater.* **174**, 40 (1997).
  - [12] J. Thomassen, F. May, B. Feldmann, M. Wuttig, and H. Ibach, *Phys. Rev. Lett.* **69**, 3831 (1992).
  - [13] D. Li, M. Freitag, J. Pearson, Z. Q. Qiu, and S. D. Bader, *Phys. Rev. Lett.* **72**, 3112 (1994).
  - [14] W. Pitsch, *Philos. Mag.* **4**, 577 (1959).
  - [15] C. M. Wayman and H. K. D. H. Bhadeshia, in *Physical Metallurgy*, 4th ed., edited by R. W. Cahn and P. Haasen (North-Holland, Amsterdam, 1996), Vol. 2, p. 1507.
  - [16] *CRC Handbook of Chemistry and Physics*, 78th ed., edited by D. R. Lide and H. P. R. Frederikse (CRC Press, Boca Raton, 1997).
  - [17] J. Giergiel, J. Shen, J. Woltersdorf, A. Kirilyuk, and J. Kirschner, *Phys. Rev. B* **52**, 8528 (1995).
  - [18] A. Biedermann, M. Schmid, and P. Varga, *Phys. Rev. Lett.* **86**, 464 (2001).
  - [19] M. Aldén, S. Mirbt, H. L. Skriver, N. M. Rosengaard, and B. Johansson, *Phys. Rev. B* **46**, 6303 (1992).
  - [20] T. Detzel, M. Vonbank, M. Donath, and V. Dose, *J. Magn. Magn. Mater.* **147**, L1 (1995).
  - [21] C. Zener, in *Phase stability in metals and alloys*, edited by P. S. Rudman (McGraw-Hill, New York, 1967), p. 25.
  - [22] H. Hasegawa and D. G. Pettifor, *Phys. Rev. Lett.* **50**, 130 (1983).